RSC Advances

ROYAL SOCIETY OF CHEMISTRY

www.rsc.org/advances

RSC Advances

RSCPublishing

Article

Microfluidic Fabrication of Multiaxial Microvessels via Hydrodynamic Shaping

Cite this: DOI: 10.1039/x0xx00000x

Michael A. Daniele[a], Kathryn Radom[b], Frances S. Ligler[c] and André A. Adams[a,*]

Received 00th January 2014,
Accepted 00th January 2014

DOI: 10.1039/x0xx00000x

www.rsc.org/

[a]Center for Bio/Molecular Science and Engineering, U.S. Naval Research Laboratory, 4555 Overlook Ave. SW, Washington D.C. 20375, USA
[b]Naval Research Enterprise Internship Program, U.S. Naval Research Laboratory, 4555 Overlook Ave. SW, Washington D.C. 20375, USA
[c]Department of Biomedical Engineering, University of North Carolina Chapel HIll and North Carolina State University, Raleigh, North Carolina 27695, USA

*Author to whom correspondence should be addressed; e-mail: andre.adams@nrl.navy.mil

Table of Contents Entry

Fabrication of small, hydrogel microvessels (*radii* < 250 um) through hydrodynamic shaping and photoinitiated polymerization is demonstrated. Photopolymerized hydrogel microvessels were produced and examined. The process is modular and amenable to generating an array of microvessel sizes and shapes.

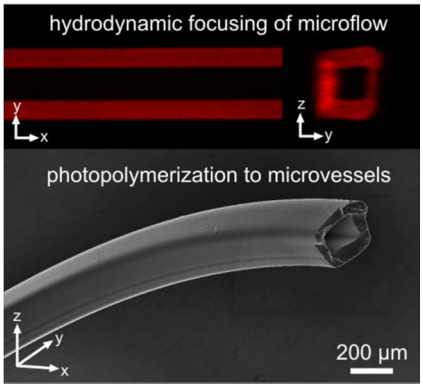

Abstract

A microfluidic fiber fabrication device was developed to prepare multiaxial microvessels with defined architecture and material constituency. Hydrodynamic focusing using passive wall structures directed biologically relevant macromer solutions into coaxial flow patterns, which were subsequently solidified via photopolymerization. Solid, coaxial, and triaxial microfibers as well as microtubes were generated from the multiaxial flows composed of both synthetic macromers and biomacromolecules.

Introduction

Biological microvessel networks, such as the cardiovascular, lymphatic, nasolacrimal and mammary systems, are important for shuttling small volumes of liquid through the human body. These tubular tissue structures have walls made of coaxial layers of different cell types supported within extracellular matrix proteins and biopolymers.[1] Mimicking the coaxial organization of cells and extracellular matrix components of these tissue microvessels is a critical goal of regenerative medicine and *in vitro* tissue engineering;[2] therefore, it is very important to develop a simple, cytocompatible process to prepare biohybrid free-standing microvessels with relatively small wall thickness (<150 µm) and varied, biomaterial composition. The reduced wall-thickness (<150 µm) is a critical parameter to avoid the formation of solute gradients in the encapsulation matrix, providing for uniform diffusion of nutrients and oxygen through the cell matrix.[3, 4]

Creation of micro-scale materials has spurred a number of diverse microfabrication techniques to generate multi-layered, cell-laden microfibers and microtubes. Unfortunately, the cytocompatible methods have required complex cell-seeding protocols and manual rolling of polymer films, and these methods are only viable for the production of large diameter tubes (>500 µm) with limited aspect ratios.[5-7] Microfluidic materials synthesis has recently emerged as a viable method for directing the placement of encapsulated cells by focusing fluid flows.[8-11] Takeuchi *et al.* recently illustrated the possibilities of hydrodynamic shaping by producing cell and protein-laden microthreads, in which a microfluidic device with concentric capillaries was constructed to organize cells and protein suspensions along a fiber axis.[11] Although promising, this "concentric-microchannel device" and often utilized alginate matrix system possesses engineering limits to the number of concentric layers.[8, 9, 11] To generate a multilayer vessel with a "concentric-microchannel device", an additional microchannel has to encase the central channel for each subsequent layer. This design requires both increased fluid volumes (as the overall device diameter increases) and increasingly fine machining of the microchannels. The ubiquitous use of alginate limits the number of concentric layers, because it relies on calcium ion diffusion for crosslinking, which could result in both uneven solidification (outer crust) and cell cytotoxicity during the lengthy time required for crosslinking.

Alternatively, a passive core-sheath microflow design would provide a better level of control and modularity required to produce cytocompatible multilayered microvessels from an array of materials. The only report of hollow polymer microvessels produced by microflow shaping utilizes the laminar flow of a photo-curable fluid and liquid template (non-polymerizing fluid), which spontaneously form concentric jet streams in certain equilibrium states.[12] The formation of the jet streams is strongly connected to the spreading coefficients of the fluids and the downstream evolution time in the microfluidic system. Accordingly, a very narrow range of conditions for jetting and fiber formation exist, otherwise droplets or wetting occurs. The shear stress in flow is greatest at the walls and immiscible interfaces, the shear forces required to form the jet streams may adversely affect any resident cell population.[13, 14] More importantly, this methodology requires a non-aqueous sheath fluid and the report states the use of a surely cytotoxic concentration of photoinitiator (8 wt.%). Consequently, the control of microfiber size and shape is coupled to material characteristics which limit the range of cytocompatible materials. With these constraints in mind, the ideal fabrication platform for the generation of multi-layered microvessels would be a combination of cytocompatible and modular microfluidic methods, *i.e.* a system in which concentric microflows are passively shaped and additional layers of polymer scaffold and cells can be trivially incorporated onto the microstructure independent of materials and cell type and population.

Herein, we report a strategy to fabricate multiaxial microfibers and microtubes using the combination of hydrodynamic shaping and *in situ* photopolymerization. We have previously developed a cytocompatible, microfluidic method to prepare microfibers with "on-the-fly" photopolymerization.[15, 16] We found that hydrodynamic shaping and photoinitiated polymerization produced minimal cellular stressors, and with the appropriate macromer system, we were able to generate biohybrid microfibers with cell viability >90%.[15, 17] Therefore, we pursued the development of a microfluidic device to generate coaxial microfibers and microtubes to mimic biological microvessels. In this design, surface features directly milled into the microchannel walls focus the multi-layered, laminar fluid flow to generate concentric fluid regimes. By combining this hydrodynamic shaping with *in situ* photopolymerization, we can continuously generate multiaxial microvessels, while avoiding the limitations of the "concentric-needle" microfluidic devices and the bio-"incompatibility" of previously reported microfluidic methods.

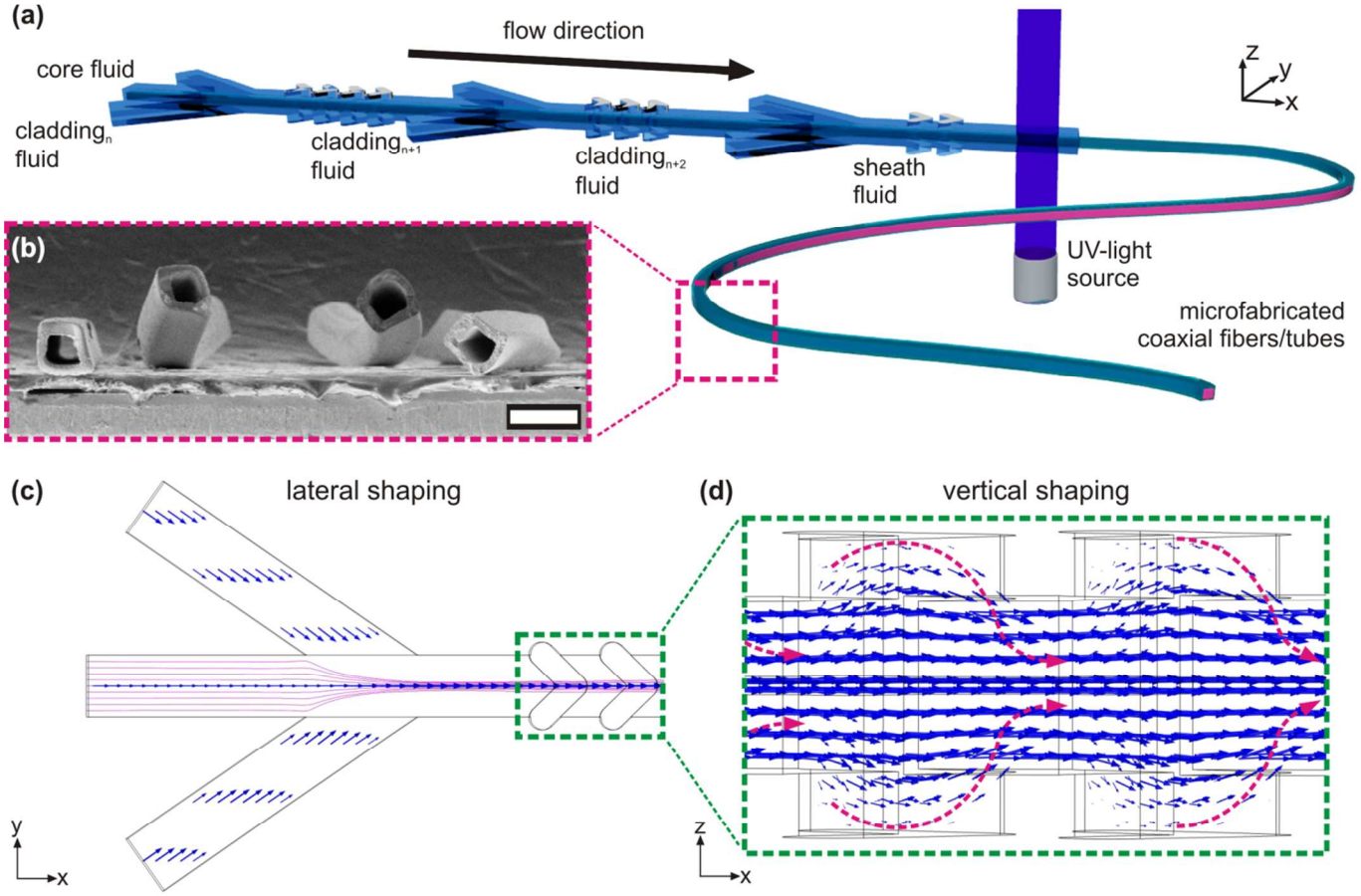

Figure 1. Schematic illustration of the design and operating mechanism of a coaxial microvessel fabrication device are shown. (a) A layout of the microchannel, showing inlet channels for core, multiple cladding fluids, and sheath fluid with successive shaping regions (not to scale). A core fluid is introduced in-line with the channel (x-axis), while successive cladding and sheath fluids are introduced at 45° through the x-y plane. After addition of the sheath fluid and upon traversing the final shaping region, exposure to UV-light solidifies the macromer-based cladding solutions into microvessels. (b) A scanning electron micrograph of a sectioned hollow microtube exhibit the representative morphology of the solidified vessels. Scale bar is 500 μm. (c) The impinging cladding and sheath fluid laterally shape the core fluids, as shown by calculated streamlines. (d) In the shaping regions, passive features (chevron-shaped grooves) milled into the microchannel walls vertically direct the core toward the center of the channel, as shown by calculated vector plots of a net streamline displacement following a two successive chevron features (hash lines are for visualization aid). The ultimate shape is controlled by the number of chevrons and fluid flow rates.

Results and Discussion

Figure 1 illustrates the design and operating mechanism of the hydrodynamic shaping microchannel for producing microvessels. The basic unit of the microfluidic device consists of three inlet channels, converging on a central channel and one shaping region. The inlet channels are used to flow reagents that will form the concentric layers of the microflow. The central microchannel then leads to the modular focusing region. The focusing region of the microchannel is patterned with chevron-shaped grooves in the top and bottom channel walls. Additional inlets and shaping regions can be directly appended onto the outlet of the microchannel to produce nested layers of fluid flow, *e.g.* a hollow or two-layer coaxial microfiber would require two shaping regions and a tetra-axial microfiber would require four shaping regions. In Figure 1b, an exemplary micrograph of a sectioned hollow microtube is shown to illustrate the uniformity of structure which is realized throughout the continuous production of meters of microvessels (*cf.* Figure S1). This microfluidic design utilizes hydrodynamic shaping to generate laminar flow in which a prepolymer solution (core or cladding fluid) and template fluid (sheath fluid) are directed into concentric flow regimes. Hydrodynamic focusing at the inlet channels sets the lateral dimension of the focused fluid (*cf.* Figure 1c), while the chevron grooves induce advection which sets the vertical dimension of the focused fluid (*cf.* Figure 1d). These hydrodynamic shaping systems have been shown to induce minimal shear stress at the center of the channel,[18] where the fluid may be carrying suspended cell populations or fragile biomacromolecules.

To design the microfabrication device and visualize the hydrodynamic shaping, computational fluid dynamics was used to simulate fluid flow. **Figure 2** shows the normalized concentration profiles for different microchannel designs. The fluid profiles were independently shaped by the fluid flow-rate ratios and number of shaping features. Two-dimensional cross-sections of the flow deformation show lateral and vertical displacement induced by the cladding fluid and shaping features. Introduction of the fluid into the channels laterally focuses the core fluid into a thin vertical stripe which spans the height of the channel. The lateral displacement of the fluids increased with an increase in the flow rate of the cladding fluid, relative to the core fluid. Figure 2 a*(i)* and Figure 2 a*(iv)* show the effective compression of the core fluid by the cladding fluid with core:cladding$_1$:sheath flow rates of 7.5:30:60 μL·min^{-1} and 7.5:15:60 μL·min^{-1}, respectively. The flow rates used were approximated using simulations then determined practically within the microfluidic system; however, the critical determinant of the flow profile is the flow rate ratios, *i.e.* 7.5:30:60 μL·min^{-1} = 1:4:8. The variation in these ratios determines the profile and general size of the resultant fibers.[15, 16, 18-20] When the laterally-focused fluid entered the shaping region, each chevron generated a rotational flow in each quadrant of the channel cross-section (*cf.* Figure 1d), such that the core fluid was separated from the top and bottom of the microchannel by the cladding fluid. The degree of vertical displacement of the core fluid was determined by the number of chevrons and increased with the increasing number of shaping features. The initial core flow can contain macromer fluid or a template fluid to create coaxial microfibers or hollow microtubes. Figure 2b*(iii)* and Figure 2b*(ix)* clearly illustrate the effect of the number of chevrons on the vertical displacement of the fluid flow. If the microchannel is designed with 3 sets of 4 chevrons, the initial core fluid will pass through 12 chevrons, compounding the vertical displacement and causing a "dog-bone" shape. The total core and cladding flow remains approximately rectangular when the width is relatively small, but begins to develop large lobes as the vertical displacement (chevron induced) becomes disparate from the lateral displacement (flow-rate ratio dependent). By tailoring the shaping regions to have 4+3+2 chevrons, the resultant flow has only passed through nine chevrons and a more symmetric flow profile is maintained (*cf.* Figure 2b*(xii)*). Within limits, the height and width of the sample stream can be controlled independently. Because height is a function of the number of chevrons and not the flow ratio as in the previous design, a designer must choose an appropriate channel dimension and chevron number. Although the vertical deflection of the fluid increases with subsequent chevrons, symmetric sample streams can be maintained by balancing the effect of flow-rate ratios with the effect of the chevrons.

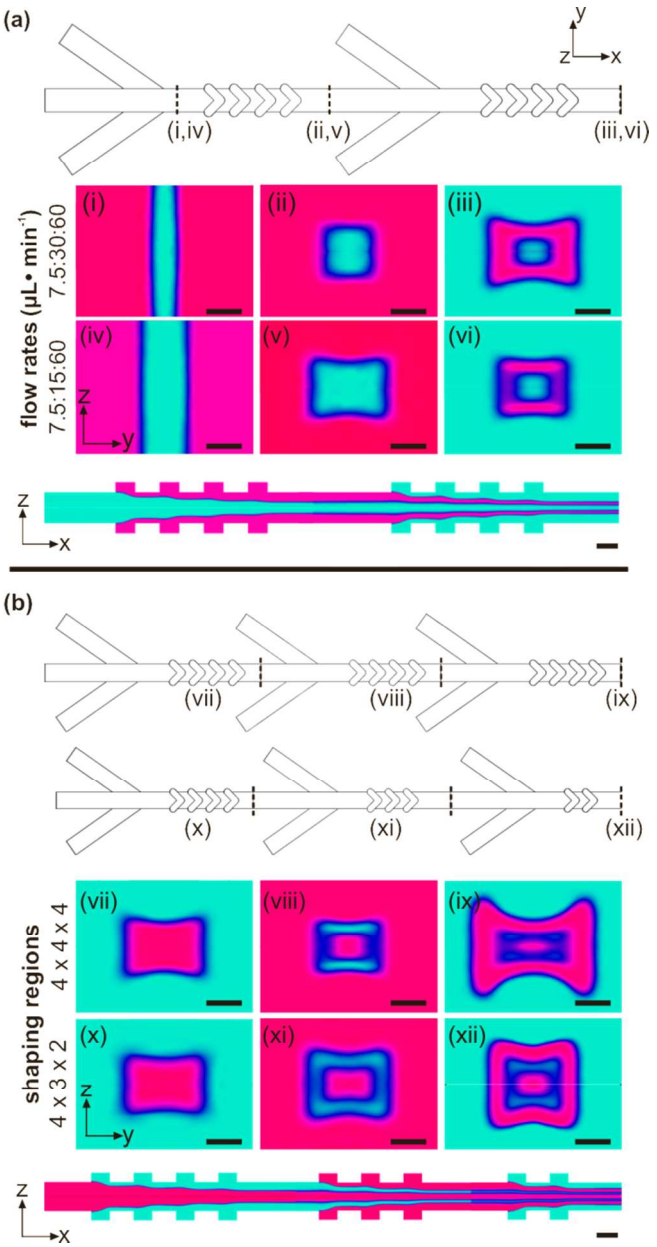

Figure 2. Finite element analysis of fluid transport and convection in microchannels. (a) A microchannel designed to produce solid microfibers, hollow and coaxial microvessels illustrates the lateral shaping effect of varied flow-rate ratios. (b) Microchannels designed to produce triaxial microvessels illustrate the compounding effect of successive shaping regions. Color variations illustrate concentration and diffusion profiles of macromer flow. For z-y cross-sections (i-xii), the scale bar is 200 μm. For z-x cross-sections, the scale bar is 500 μm).

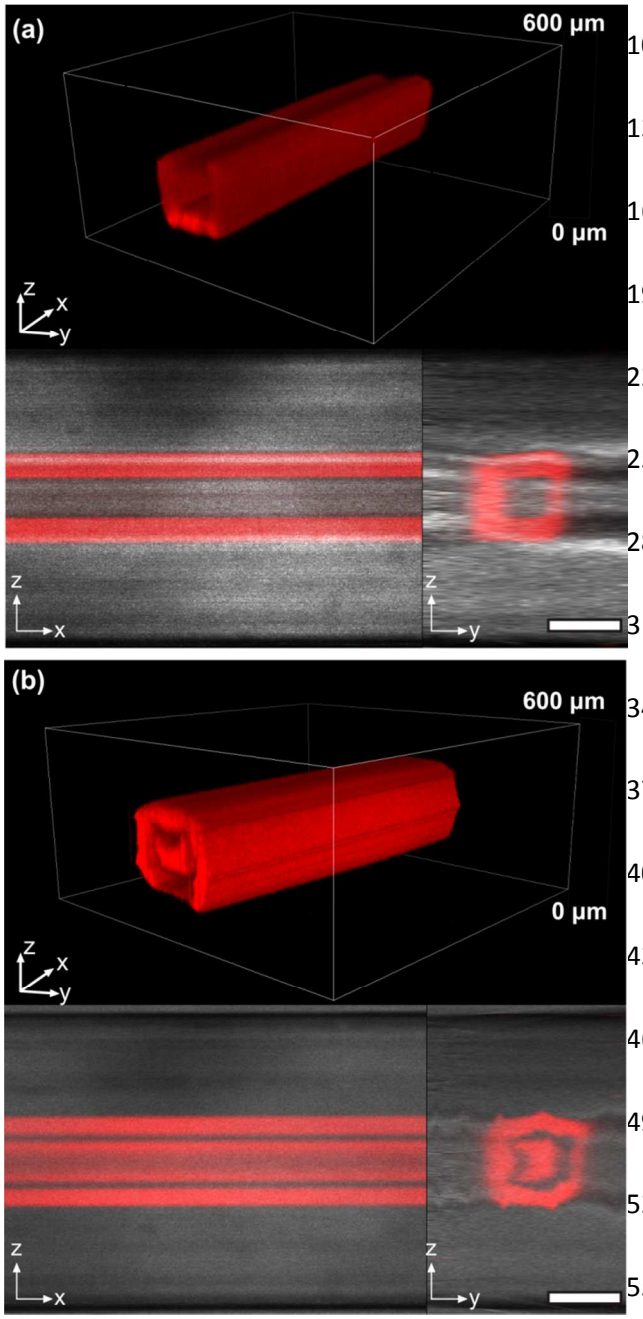

Figure 3. Laser scanning confocal micrographs of the fluid flow cross-section from channels with varying shaping feature architectures: (a) 4+4 chevrons and (b) 4+3+2 chevrons. The core:cladding$_n$:sheath flow rates for (a) and (b) are 7.5:15:60 and 7.5:15:60:120 µL•min-1. Scale bars are 250 µm.

Prior to the fabrication of microvessels, the flow profiles were characterized by laser scanning confocal microscopy (LSCM). Based on the fluid dynamics simulations, we could rationally determine that the 4+4 and 4+3+2 devices would produce the most symmetric fluid flows, so these microchannel designs were fabricated and tested. **Figure 3** shows LSCM micrographs of the microflow cross-section resulting from microfabrication of device designs with two or three shaping regions, 4+4 and 4+3+2 chevrons, respectively. The "real-time" fluid flow develops in coordination with the calculated laminar Navier-Stokes flow, as evidenced by comparison with the concentration cross-sections (*cf.* Figure 2). The core:cladding$_n$:sheath flow rates used for the 4+4 chevron device were 7.5:15:60 µL·min^{-1}, and the flow rates for the 4+3+2 chevron device were 7.5:15:60:120 µL·min^{-1}. By composing consecutive inlets and shaping regions, we clearly attained concentric layers of cladding macromer flow, which can be solidified into coaxial microfibers or microtubes.

Hydrogel microvessels were generated by the photopolymerization of macromer solutions introduced into the microfabrication device. The non-cytotoxic macromers selected were poly(ethylene glycol) dimethacrylate (PEGDMA) and gelatin. Aqueous PEGDMA solutions (50 wt.%) were solidified by photoinitiated free-radical polymerization with the use of the cytocompatible and water soluble photoinitiator, 2-hydroxy-4-(2-hydroxyethoxy)-2-methylpropiophenone (I2959).[21] A minimal concentration of 0.5 wt.% was used to crosslink the PEGDMA and generate the microvessels. The UV light intensity delivered to the channel surface was *ca.* 10 mW·cm^{-2} (a dose of 4-9 mJ, depending on flow rates). Aqueous sheath solutions were composed of poly(ethylene glycol) (PEG_{400}). All PEGDMA and PEG_{400} solutions were prepared at 50 wt.% in phosphate buffered saline (0.1 M, pH=7.4). PEGDMA was chosen as the foundation material of the microfiber and microtubes because of its extensive use in biomaterial formulations. Gelatin was utilized as a representative extracellular matrix protein within the filled multiaxial microfibers. In low concentrations, gelatin is water soluble and has been shown to be an excellent support for 3D tissue culture.

Figure 4 illustrates a sample of the characteristic microvessels that can be obtained with such a device. Exposure of poly (ethylene glycol) dimethacrylate macromer solutions to UV-light initiates crosslinking and solidifies the resultant microfiber or microtube (*cf.* Figure 4a). A window in the device approximately 2 cm long was exposed to 365 nm irradiation (10 mW·cm^{-2}), resulting in an estimated dose of <10 mJ·cm^{-2}. This dose was enough to crosslink mechanically stable microvessels that could be handled for characterization. Of course, dosage can be tuned to attain desired crosslink densities or to meet other desired reaction conditions. This would be simply achieved by adjusting the light intensity or residence time. A comparable dosage was shown to be benign while encapsulating endothelial cells within microfibers,[17] and even higher dosing has been used to produce viable encapsulated cell populations.[21]

Scanning electron micrographs (SEM) show both multiaxial microfibers and microtubes can be produced in concurrence with fluid dynamics simulations (*cf.* Figure 2) and flow visualizations (*cf.* Figure 3). Initially, solid microfibers were fabricated with a 4 x 4 device and core:cladding$_n$:sheath flow rates of 7.5:15:120 µL·min^{-1} (*cf.* Figure 4b). PEGDMA solutions were used for the core and cladding to form a uniform microfiber. The sheath fluid sets the final shape of the microvessel; moreover, it ensured the macromer solutions were separated from the microchannel wall so photopolymerization did not cause clogging. Addition of concentric cladding layers was achieved by either the incorporation of secondary macromer solutions (coaxial microfibers, *cf.* Figure 4d) or the addition of consecutive shaping regions (triaxial microfibers, *cf.* Figure 4e). In these variants, the core solution was replaced with a PEG_{400} or gelatin solution (20 wt.%), which produced hollow microvessels and coaxial microfibers, respectively (*cf.* Figure 4 c,d). Introduction of macromer-free PEG_{400} template fluid resulted in capillary-like microvessels with uniform wall thicknesses (<100 µm) and diameters (<500 µm). The thin, uniform walls are ideal for any future incorporation of a cell population; moreover, the hollow microtubes were physically robust and could withstand continued

manipulation. The hollow microvessels showed average inner and outer diameters of 125 µm and 200 µm, respectively with wall thicknesses that were 75 µm or less. For reference, vascular vessel systems range from outer diameters of 1.5 cm (elastic arteries) to inner diameters less than 2 µm (capillary) with wall thicknesses everywhere in between. Accordingly, these microfluidic fabrication techniques can provide a bridge between generating large, mechanically robust vessels and capillary structures.

The simple incorporation of an ECM protein illustrated the potential for facile generation of a suitable cell culture environment within the microvessel. For the production of coaxial biohybrid fibers, gelatin was simply dissolved into the core fluid, and by adjusting the fluid flow rates, we could develop small and large, microvessels incorporating gelatin into either the lumen or the walls (*cf.* Figure 4c). The resultant fiber represents a cytocompatible environment for cell-proliferation and tissue construction. The combination of ECM proteins and PEG with encapsulated endothelial cells have been shown to produce cell-laden microfibers with a comparable system.[17]

Lastly, we incorporated a successive shaping region to generate triaxial microfibers (*cf.* Figure 4d). The triaxial microfibers are composed of three layers, from inside to outside: PEGDMA, gelatin, PEGDMA. The gelatin cladding layer was reduced to 5 wt.% in an attempt to generate a "bull's eye"-like geometry, in which a cladding layer would behave as the vessel. Although the triaxial microfibers were delicate and required careful preparation to image, it is clear that the triple layered flow was generated and could be solidified into a triaxial microfiber.

All microvessels were produced continuously and collected in a water-bath. Solid and hollow hydrogel microvessels maintained robust geometric profiles in both the swollen and dehydrated states. When swollen, the soft ECM protein maintained its geometric profile, while freeze-drying for characterization resulted in phase-separation and some fiber deformation. Each variant exhibited reproducible size and shapes over meter lengths (*cf.* Figure SI1).

Experimental Section

Materials: PEGDMA (M_W = 750), Gelatin, Type A (from bovine skin), and Irgacure 2959 were purchased from Sigma Aldrich (St. Louis, MO). Prior to mixing macromer solutions, the hydroquinone inhibitor was removed from the PEGDMA using an inhibitor removal column (column SDHR-4 from Scientific Polymer Products, Inc., Ontario, NY). Gelatin methacrylamide was synthesized according to previous methods. The PEGDMA macromer solution was prepared by mixing PEGDMA (50 wt.%) and I2959 (1 wt.%) in PBS and heating at 70 ºC until dissolved. The GelMA macromer solution was prepared by mixing GelMA with PBS and heating at 37 ºC until dissolved. The sheath solution was prepared by mixing PEG (M_W = 400) (50 wt.%) with PBS. PBS solutions (pH = 7.4, 0.1M) were prepared with deionized water obtained from a Millipore Sapphire System and exhibited a resistivity of *ca.* 10^{18} ohm^{-1} cm^{-1}.

The microfluidic devices were direct milled from poly(methyl methacrylate) (PMMA) or cyclic-olefin-copolymer (COC) for confocal microscopy and fiber fabrication, respectively. The devices channels were 1.0 mm x 0.75 mm (width x height) with chevron features that were 0.375 mm x 0.250 mm (width x depth). Detailed schematics of both the confocal and production device are presented in the Supplementary Information (*cf.* Figure S2).

Computational Models: All simulations in this work were carried out using the COMSOL Multiphysics (COMSOL, Inc., Burlington, MA) computational tool. Steady-state solutions of incompressible Navier–Stokes flow were coupled with concentration-diffusion calculations to investigate the profile of the core stream. A single-phase, Newtonian fluid was assumed. The low molecular weight macromer solutions should not exhibit significant non-Newtonian behavior until after crosslinking is photoinitiated. An adaptive solver was used to obtain an optimized mesh density. The flow field velocity was solved first for each simulation, and the obtained solution was used to calculate the concentration profile of the fluids in the system, producing an image of the cross-section of the core stream. Calculations were carried out for different flow-rate ratios between the sheath and sample streams. An adaptive solver was applied to obtain an optimized mesh for concentration-diffusion calculations. Taking advantage of the symmetric design of the device, only half of the channel was modeled to reduce processing times, and presented results are mirrored across the latitudinal axis.

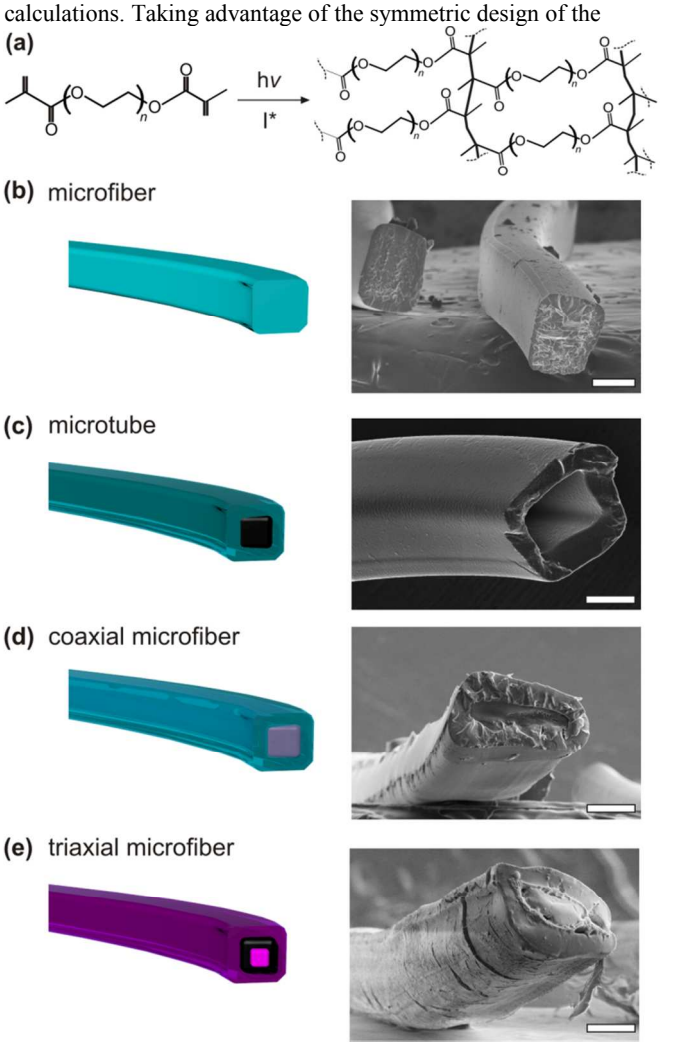

Figure 4. Demonstration of continuous hydrodynamic shaping and microvessel production with different multiaxial architectures. (a) Hydrogel microvessels were produced by photopolymerization of poly(ethylene glycol) dimethacrylate. Scanning electron micrographs of (b) solid microfibers, (c) hollow, (d) coaxial and (e) triaxial microvessels. Scale bars are 150 µm.

Laser Scanning Confocal Microscopy: LSCM imaging of the hydrodynamic shaping process were obtained with a Nikon TE2000 Inverted Confocal Microscope. Core, cladding and sheath fluids composed of poly(ethylene glycol) and gelatin were used to simulate

the flow of macromer solutions. The appropriate fluid was dyed with rhodamine-B to produce the fluorescent flow.

Preparation of coaxial microfibers and microtubes: In a typical microfiber fabrication, the aqueous macromer solutions were introduced to the microchannel from the inside-out, *i.e.* the core solution was introduced first, followed by the series of cladding solutions, and finally the sheath was introduced to the microchannel. All fluids were injected into the microchannel with syringe pumps. Careful attention was paid to fluid flow in the chevrons to ensure the passage of any trapped air bubbles. The microchannel was suspended vertically over an aqueous collection bath. The photopolymerization reaction induced by UV light exposure was used to continuously solidify the microfibers and microtubes. Regions of hydrodynamic shaping were blocked from UV-light to avoid premature crosslinking and subsequent clogging. The device is vertically suspended, and the microchannel exit was submerged in an aqueous collection bath. As the microfibers and microtubes are solidified, they are ejected into the aqueous collection bath, rinsed with water and then lyophilized for storage.

Characterization: Hydrodynamic shaping of the fluid streams was observed with a laser scanning confocal microscope (Nikon). Detailed microfiber and microtube structures were observed by scanning electron microscopy (LEO Supra55, Karl Zeiss Inc., Peabody, MA). Microscopy samples were lyophilized and sputter coated with ~6 nm of gold (Cressington Auto 108 Sputter Coater, Ted Pella Inc., Redding, CA).

Conclusions

A microfluidic microfabrication device was developed to prepare multiaxial microvessels with defined architecture and material constituency. Hydrodynamic focusing using passive wall structures directed macromer solutions into coaxial flow patterns, which were subsequently solidified *via* photopolymerization. By utilizing computational fluid dynamics simulations, the architecture of the microvessel could be accurately predicted. From these calculations, the size and symmetry of the microvessel architectures were tailored by adjusting the core:cladding$_n$:sheath fluid flow rates, and the modular addition of concurrent shaping regions resulted in the multiaxial architectures. Solid, coaxial, triaxial microfibers and microtubes were easily generated from the multiaxial flow, while both synthetic macromers and biomacromolecules were utilized to illustrate the types of tubular structures that can be crafted.

Ultimately, this modular microfluidic strategy, and our ability to precisely and continuously produce multi-axial fibers provide a new method to address the specific requirements for engineering of biologically relevant microstructures, such as capillaries and lymph vessels. Since the shaping process is adaptable to aqueous macromer solutions, we intend to explore a range of popular bio-derived materials, such as gelatin methacrylamide,[22] collagen,[23] and hyaluronic acid[24] to develop different bioactive microvessels. We believe that the synergy of this microfabrication design and novel biomaterials will be useful for 3D cell culturing and tissue engineering applications that incorporate heterotypic cell cultures about the microvascular networks.

Acknowledgements

Work performed by Michael A. Daniele was supported by a National Research Council Postdoctoral Fellowship. Work performed by Kathryn Radom was supported by the Naval Research Enterprise Internship Program (NREIP). This work was supported by the Naval Research Laboratory (NRL) and the Office of Naval Research (ONR) 6.1 work unit MA041-06-41-9899. The views expressed within represent those of the authors and do not reflect the opinion or policy of the U.S. Navy or Department of Defense.

Supporting Information

Electronic Supplementary Information (ESI) available: [details of any supplementary information available should be included here]. See DOI: 10.1039/c000000x/

References

1. M. H. Ross and P. Wojciech, *Histology: A Text and Atlas, 6th Ed.*, Lippincott Williams & Wilkins, Philadelphia, PA, 2010.
2. L. G. Griffith and M. A. Swartz, *Nature Reviews Molecular Cell Biology*, 2006, **7**, 211-224.
3. H. Geckil, F. Xu, X. H. Zhang, S. Moon and U. Demirci, *Nanomedicine-Uk*, 2010, **5**, 469-484.
4. N. W. Choi, M. Cabodi, B. Held, J. P. Gleghorn, L. J. Bonassar and A. D. Stroock, *Nat Mater*, 2007, **6**, 908-915.
5. B. Yuan, Y. Jin, Y. Sun, D. Wang, J. S. Sun, Z. Wang, W. Zhang and X. Y. Jiang, *Adv Mater*, 2012, **24**, 890-+.
6. N. Asakawa, T. Shimizu, Y. Tsuda, S. Sekiya, T. Sasagawa, M. Yamato, F. Fukai and T. Okano, *Biomaterials*, 2010, **31**, 3903-3909.
7. B. J. Papenburg, J. Liu, G. A. Higuera, A. M. C. Barradas, J. de Boer, C. A. van Blitterswijk, M. Wessling and D. Stamatialis, *Biomaterials*, 2009, **30**, 6228-6239.
8. K. H. Lee, S. J. Shin, Y. Park and S. H. Lee, *Small*, 2009, **5**, 1264-1268.
9. M. Hu, R. S. Deng, K. M. Schumacher, M. Kurisawa, H. Y. Ye, K. Purnamawati and J. Y. Ying, *Biomaterials*, 2010, **31**, 863-869.
10. S. Fleischer, R. Feiner, A. Shapira, J. Ji, X. Sui, H. D. Wagner and T. Dvir, *Biomaterials*, 2013, **34**, 8.
11. H. Onoe, T. Okitsu, A. Itou, M. Kato-Negishi, R. Gojo, D. Kiriya, K. Sato, S. Miura, S. Iwanaga, K. Kuribayashi-Shigetomi, Y. T. Matsunaga, Y. Shimoyama and S. Takeuchi, *Nature Materials*, 2013, **12**, 6.
12. C. H. Choi, H. Yi, S. Hwang, D. A. Weitz and C. S. Lee, *Lab Chip*, 2011, **11**, 1477-1483.
13. Y. Chisti, *Critical Reviews in Biotechnology*, 2001, **21**, 67-110.
14. W. W. Hu, C. Berdugo and J. J. Chalmers, *Cytotechnology*, 2011, **63**, 445-460.
15. M. A. Daniele, S. H. North, J. Naciri, P. B. Howell, S. H. Foulger, F. S. Ligler and A. A. Adams, *Advanced Functional Materials*, 2013, **23**, 698-704.
16. A. L. Thangawng, P. B. Howell, C. M. Spillmann, J. Naciri and F. S. Ligler, *Lab Chip*, 2011, **11**, 1157-1160.
17. M. A. Daniele, A. A. Adams, J. Naciri, S. H. North and F. S. Ligler, *Biomaterials*, 2014, **35**, 1845-1856.
18. A. R. Shields, C. M. Spillmann, J. Naciri, P. B. Howell, A. L. Thangawng and F. S. Ligler, *Soft Matter*, 2012, **8**, 6656-6660.
19. D. A. Boyd, M. A. Daniele, A. A. Adams and F. S. Ligler, *Journal of Visualized Experiments*, 2014, **83**, e50958.
20. A. L. Thangawng, P. B. Howell, J. J. Richards, J. S. Erickson and F. S. Ligler, *Lab on a Chip*, 2009, **9**, 3126-3130.
21. C. G. Williams, A. N. Malik, T. K. Kim, P. N. Manson and J. H. Elisseeff, *Biomaterials*, 2005, **26**, 1211-1218.

22. M. Nikkhah, N. Eshak, P. Zorlutuna, N. Annabi, M. Castello, K. Kim, A. Dolatshahi-Pirouz, F. Edalat, H. Bae, Y. Z. Yang and A. Khademhosseini, *Biomaterials*, 2012, **33**, 9009-9018.
23. L. A. Micol, M. Ananta, E. M. Engelhardt, V. C. Mudera, R. A. Brown, J. A. Hubbell and P. Frey, *Biomaterials*, 2011, **32**, 1543-1548.
24. J. A. Burdick and G. D. Prestwich, *Adv Mater*, 2011, **23**, H41-H56.